The Preparation of a Lignosulfonate/Chitosan–Graphene Oxide Hydrogel Biosorbent to Effectively Remove Cr(VI) from Wastewater: Adsorption Performance and Mechanisms

Caohui Han [1,2], Xiaonan Liu [1,2], Tingting Wang [1,2], Xiaoyin Sun [1,2], Lu Bai [1,2] and Yongchang Sun [1,2,*]

[1] School of Water and Environment, Chang'an University, Xi'an 710054, China

[2] Key Laboratory of Subsurface Hydrology and Ecological Effect in Arid Region, Ministry of Education, Chang'an University, Xi'an 710054, China

* Correspondence: ycsun@chd.edu.cn; Tel.: +86-29-8233-9952; Fax: +86-29-8233-9281

Abstract: A lignosulfonate/chitosan–graphene oxide hydrogel (LCGH) composite was successfully synthesized to effectively remove Cr(VI) from wastewater. The physical–chemical properties of the prepared LCGH was characterized by SEM, FT-IR, XRD, XPS, and TGA. The results showed that LCGH had an cross-linked three-dimensional porous network structure that was conducive to Cr(VI) adsorption, resulting in a high Cr(VI) adsorption capacity (564.2 mg/g). Thermodynamic analysis showed that Cr(VI) adsorption on LCGH was spontaneous endothermic and fitted well with the pseudo-second-order kinetic and Langmuir models. The reaction mechanisms for Cr(VI) removal were hydrogen bond, electrostatic attraction, and π-π interaction. LCGH demonstrated good reproducibility and its adsorption capacity of Cr(VI) could still maintained at 85.4% after 5 cycles of regeneration. The biosorbent LCGH was a low-cost and eco-friendly material, which has a good prospect for Cr(VI) wastewater removal.

Keywords: lignosulfonate; graphene oxide; hydrogel; Cr(VI); adsorption

1. Introduction

Cr(VI) polluted wastewater produces great harm because of its toxic and carcinogenic effects in living organisms [1]. A variety of economical and efficient means of Cr(VI) removal are available. Traditional treatment techniques include membrane filtration [2], ion exchange [3], adsorption [4], and chemical photocatalytic [5]. Among them, adsorption is a useful technology because of its convenient preparation, low cost, and widely applied of the adsorbent [6]. The preparation of adsorbents from biomass feedstock has received much attention because of their wide range of sources. For example, cellulose and its derivatives and waste straw have been developed as efficient adsorbents for environmental treatment [7,8]. However, the preparation of efficient adsorbents from biomass raw materials and its components needs investigation.

Sodium lignosulfonate (SL) is a derivative of lignin, and its structure contains carboxyl, sulfonic acid and phenolic hydroxyl groups [9], which motivates researchers to develop environment-friendly, biodegradable and reproducible materials in environmental management [10]. For example, SL was endowed with magnetism and showed excellent Cr(VI) adsorption performance (57.1 mg/g) [11]. Lignosulfonate/N-methylaniline (LSMA) composite showed a strong affinity for Cr(VI) in pH 2.0 solution and possessed good adsorption properties (1264.8 mg/g) [9]. The Cu(II) adsorption by lignosulfonate through phosphoric acid activation, showing superior adsorption performance at pH 2.0 [12]. The carbon microspheres prepared with sodium lignosulfonate, $ZnCl_2$ and polystyrene had a significant adsorption effect on Cr(VI) (227.7 mg/g) [13].

Graphene oxide (GO) has been used in many fields because of its excellent properties, especially as a composite material [14]. GO can adsorb heavy metals due to the presence

of oxygen-containing groups (hydroxyl, carboxyl, epoxy, and ketone). It can form an extended layered structure, showing the characteristics of expansion and intercalation [15,16]. Therefore, GO can be widely used to prepare materials, especially in excellent performance heavy metal adsorbents. For instance, the amino-functionalized graphene oxide (GONN) showed superior adsorption properties for Cr(VI) (1185 mg/g) [17]. Free-standing GO foam (GOF) was a special adsorbent for Zn^{2+}, Fe^{3+}, Pb^{2+}, and Cd^{2+} with a large surface area (578.4 m^2/g) [18].

Herein, chitosan (CS) has the advantages of biocompatibility and biodegradation, which attracts many researchers to use modified CS-based materials to adsorb heavy metals. For example, Sakr et al. prepared a nano-silica/chitosan (SiO_2/CS) sorbent with high adsorption capacity on uranium(VI) (165 mg/g) at pH 3.5 [19]. The functionalized chitosan/4-(2-pyridinazo) resorcinol (CS-PAR) adsorbent showed a maximum adsorption capacity of 170.23 mg/g for Cu(II) [20]. In addition, chitosan immobilised in alginate (ALG-CHz) showed good adsorption properties for Cu(II) (527.3 mg/g) and Cd(II) (207.0 mg/g) [21]. Since the structure of CS contains hydroxyl and amino groups, it can combine SL and GO through electrostatic attraction and hydrogen bonding [22], to obtain a composite material with large specific surface area, good stability, environmental friendliness, and three-dimensional structure, which is expected to have good adsorption performance for Cr(VI) in wastewater adsorption [23].

In this work, we investigated a facile and green approach to preparing an environmentally friendly lignosulfonate/chitosan-graphene oxide hydrogel (LCGH) composite and applied it to heavy metal removal from wastewater. In LCGH, SL inserted into the layers offering strong repulsion, and GO provided a multilayer skeleton, whereas CS acted as a crosslinker to maintain a stable three-dimensional network. The current study aims to: (i) investigate the influences of CS/SL/GO mass ratio, initial pH, contacting time, temperature, and initial concentration; (ii) explore Cr(VI) adsorption mechanism on LCGH; (iii) apply LCGH to the Cr(VI) removal in practical application; and (iv) investigate the recycle and reuse of LCGH.

2. Materials and Methods

2.1. Material

Sodium lignosulfonate (SL) was obtained from Yuanye Biological Technology Co., Ltd. (Suzhou, China). Chi-tosan (CS) was bought from Lanji Biological Technology Co., Ltd. (Shanghai, China). Graphene oxide (GO) was achieved from Carbon Technology Co., Ltd. (Suzhou, China). $K_2Cr_2O_7$ was bought from Beilian Fine Chemicals Development Co., Ltd. (Tianjin, China).

2.2. Synthesis of LCGH

Briefly, a solution of GO (10 mg/mL) was diluted with distilled water and ultrasonically dispersed for 1 h to get 2.5 and 1.25 mg/mL. Then SL was put into the above obtained GO solution and sonicated for 30 min to ensure uniform dispersion. Subsequently, the solution (1 mg/mL, 0.8 mg/mL) was prepared by dissolving a certain quality of chitosan (CS) in 1 wt% glacial acetic acid solution. Take 10 mL of this CS solution and slowly add dropwise to the above-mentioned mixed SL and GO solution. The corresponding CS/SL/GO mass ratios were 1:5:10, 1:10:10, 1:10:5, 2:10:10, 1:5:5. Finally, the solution was magnetically stirred, then placed in Tren nylon reactor at 180 °C (4 h). The prepared biosorbent was cleaned with distilled water and freeze-dried for subsequent use (Figure 1).
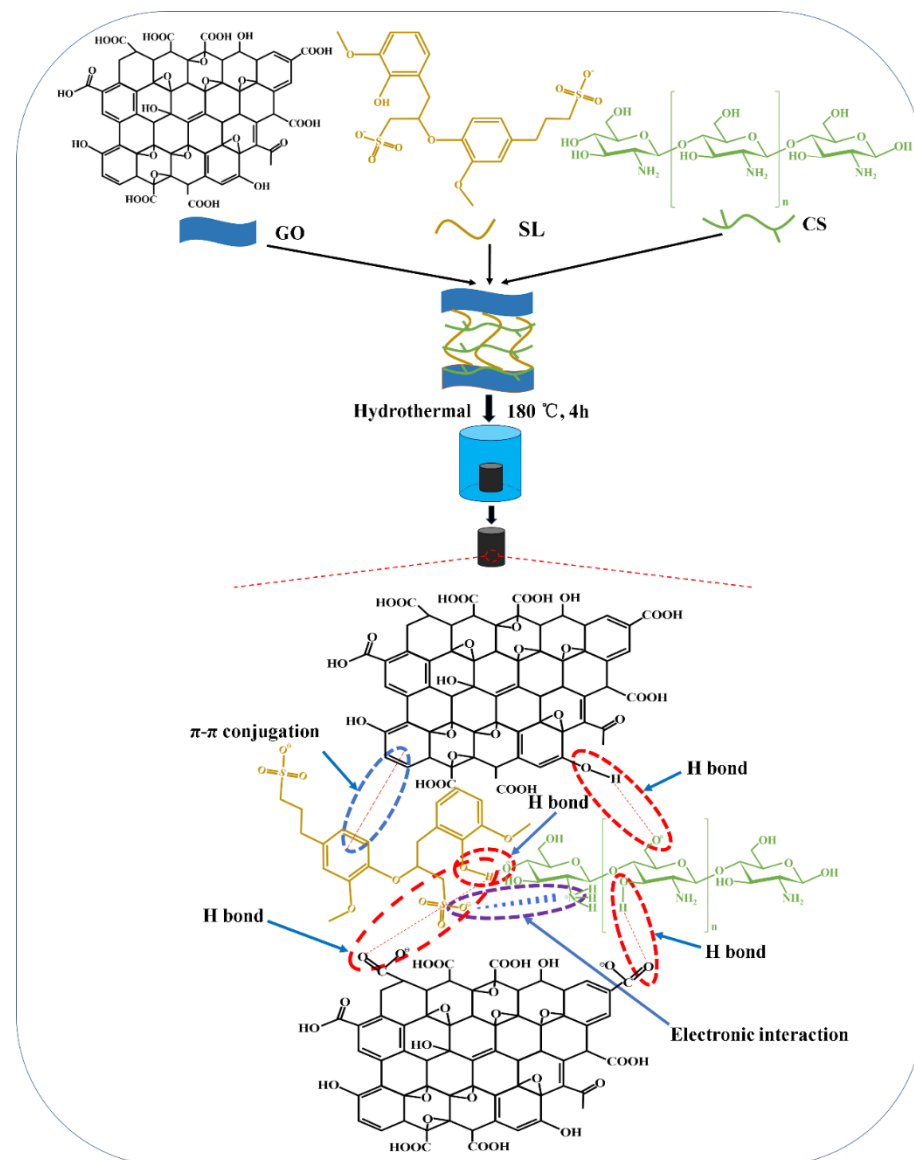
Figure 1. Preparation process of LCGH.

2.3. Characterizations

Fourier transform infrared spectroscopy (FT-IR) was identified by Bruker Tensor II (Germany). The materials surface morphology were obtained by scanning electron microscope (SEM, 20 kV, Japan). The composites were analyzed with X-ray diffraction (XRD, Bruker D8 advance, Germany) and X-ray photoelectron spectroscopy (XPS, Kratos Axis Ultra, Japan). Thermogravimetric analysis (TGA, Discovery SDT 650, Germany) was used to test the thermal stability in an inert atmosphere.

2.4. Adsorption Experiments

The adsorption capacities of Cr(VI) by LCGH were evaluated. The required Cr(VI) solution was prepared using $K_2Cr_2O_7$. The following batch processing model was generally used in the experiment: the LCGH was placed in 100 mL Cr(VI) solution, then stirred continuously at 130 rpm. The pH was adjusted to 1.0–10.0 with 0.1 M HCl or NaOH. Certain quantities of Cu(II), Zn(II) and Cu(II) + Zn(II) (1:1) were added to 50 mg/L Cr(VI) solution with mass concentration ratios of 1:1, 2:1, 3:1 and 4:1 to explore the influence of Cr(VI) adsorption in binary and ternary heavy metals systems. Then 0.2–1.8 mol/L NaCl, KCl and $CaCl_2$ inorganic salts were added to study the influence of Cr(VI) removal efficiency at

different ionic strength. The concentration of Cr(VI) was quantitatively measured using an UV-visible spectrophotometer. The adsorption capacity and removal percentage were obtained according to Equations (1) and (2):

$$q_e = \frac{(C_0 - C_e)V}{m} \tag{1}$$

$$R = \frac{C_0 - C_e}{C_0} \times 100\% \tag{2}$$

where q_e is the adsorption capacity; R is the removal percentage; and C_0 and C_e (mg/L) are the initial and equilibrium concentration, respectively; V (L) is the solution volume, and m (g) is the weight of LCGH used. All experiments were performed in duplicate. Each point represents the average of repeated measurements.

2.5. Reusability Study

The composite hydrogel with mass ratio CS:SL:GO = 1:10:10 was added to Cr(VI) solution (50 mg/L), the hydrogel was adsorbed by shaking at 130 r/min for 3 h at pH = 2.0 and 25 °C ± 0.5 °C. The adsorbed LCGH was parsed in 0.1 M NaOH (100.0 mL) to regenerate LCGH. The reuse efficiency of LCGH was calculated as follow Equation (3):

$$Reuse\ efficiency(\%) = \frac{q_n}{q_1} \times 100\% \tag{3}$$

where q_1 and q_n are the initial and nth time adsorption capacities (mg/g), respectively.

3. Results and Discussion

3.1. Characterization of LCGH

3.1.1. FT-IR

As shown in Figure 2a, the peak near 3255 cm^{-1} was due to the -OH bond stretching vibration of SL, GO, CS, and LCGH [24]. The peak at 1650 cm^{-1} was belonged to C=C stretching. The stretching vibration peaks of GO and LCGH at 1760 cm^{-1}, 1112 cm^{-1}, and 1065 cm^{-1} were the functional groups, such as carbonyl group and C-OH stretching [25]. The peaks of LCGH at 2948 cm^{-1} and 2856 cm^{-1} were -CH$_3$ and -CH$_2$ in CS and SL, respectively [26]. The new peak of LCGH at 1015 cm^{-1} originated from S=O group of -SO$_3$ in SL, and the new peaks at 1153 cm^{-1} and 1380 cm^{-1} were caused by -NH- and -C-N stretching in CS, respectively [23,27]. The peaks detected in SL, GO, and CS were all clearly characterized in LCGH, indicating that the composite was successfully prepared.

3.1.2. XPS

The XPS analysis of LCGH showed the ratios of different elements (Figure 2b). For the C element, the mass ratios for CS/GO, SL/GO, and CS/SL/GO were 1:10, 1:1, and 1:10:10, respectively. The content of C decreased from 75.19 at.% to 58.94 at.%, but the O content increased from 24.20 at.% to 38.76 at.%. The N content of the prepared hydrogel without SL was 0.61 at.%, which was due to the presence of chitosan [28]. The same S content of chitosan-free hydrogel was 0.35 at.%, which was attributed to the SL [29]. The N and S contents of the LCGH composite with CS and LS were 2.06 at.% and 0.24 at.%, which indicated that CS and SL were successfully introduced into the composite. As shown in Figure 2c–e, the contents of C-C/C=C, C-O, C=O, and O-C=O of each component material were 72.91%, 16.12%, 7.04%, and 3.93% for CS/GO (1:10); 75.62%, 12.45%, 6.99%, and 4.95% for SL/GO (1:1); and 60.00%, 23.95%, 10.53%, and 5.53% (CS/SL/GO = 1:10:10), respectively. The contents of C-O, C=O, and O-C=O on LCGH composite were higher than those composites without SL and CS addition, indicating that the introduction of both SL and CS could increase the content of oxygen, such as -OH and -COOH [30].
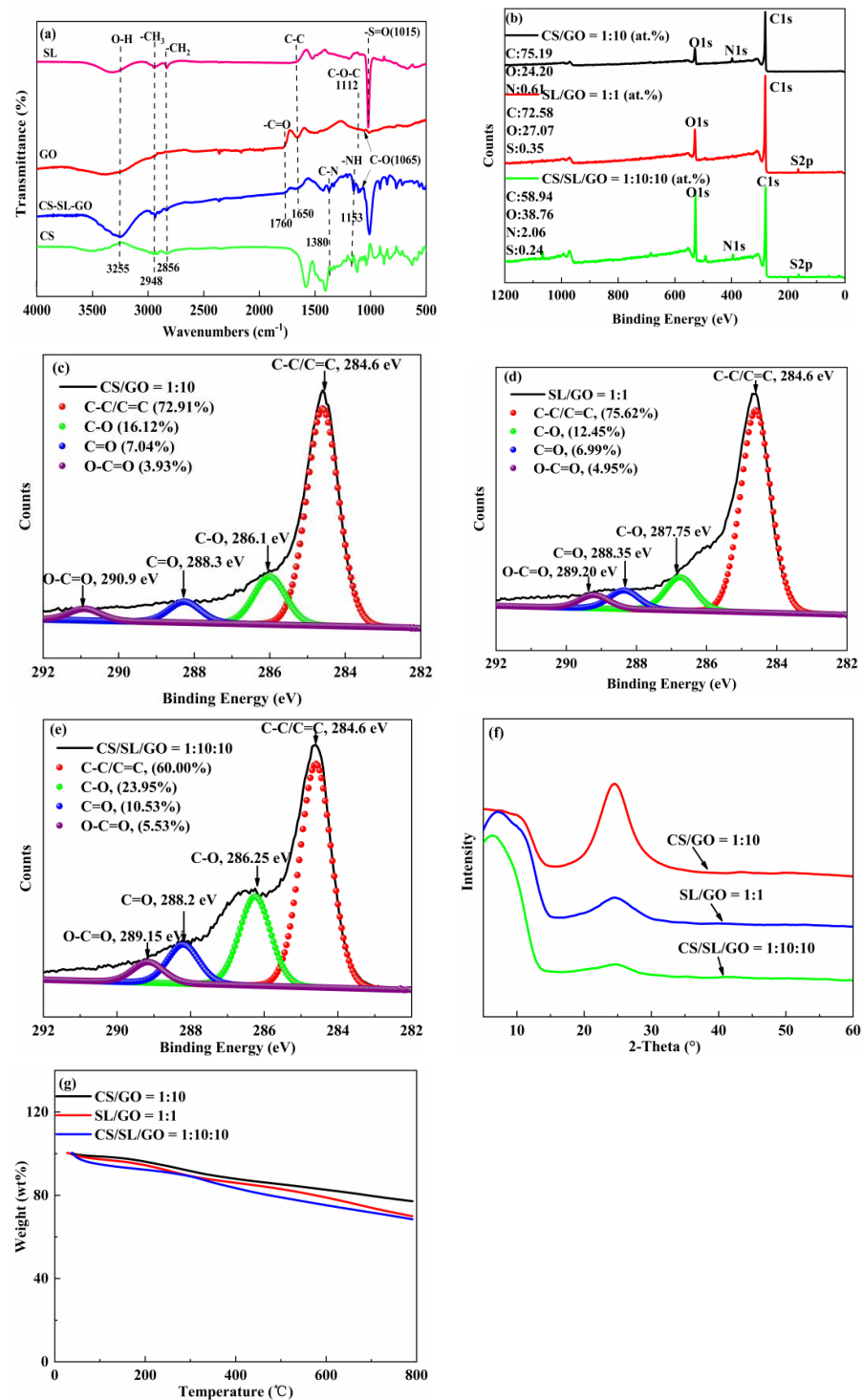
Figure 2. (**a**) FT-IR spectra of SL, GO, CS and LCGH, XPS spectra of C1s peaks for the (**b**) total spectra, (**c**) CS/GO = 1:10, (**d**) SL/GO = 1:1, and (**e**) CS/SL/GO = 1:10:10, (**f**) XRD spectra of LCGH, (**g**) TGA curves of the LCGH.

3.1.3. XRD

As shown in Figure 2f, the material CS/GO = 1:10 had a diffraction peak at 2θ = 24.44°, and the interlayer spacing calculated according to Bragg's law was 0.364 nm. The diffraction peaks of SL/GO = 1:1 and CS/SL/GO = 1:10:10 were 2θ = 24.65° (d = 0.361 nm) and 2θ = 24.37° (d = 0.365 nm), respectively. It could be seen that the addition of SL and CS increased the layer spacing of CS/SL/GO, which may have been caused by the interaction

of the GO layer when SL was inserted into CS crosslinking [15,23]. At the same time, it could be seen that the peaks displayed by CS/SL/GO were wide and weak, indicating the amorphous properties of the composite material [31].

3.1.4. TGA

The TGA curves of CS/GO, SL/GO, and CS/SL/GO composites as shown in Figure 2g. It can be observed that the initial degradation temperature of the CS/GO composite was 217.27 °C, and the maximum weight loss occurred at 330.84 °C, with mass loss of 22.84%. The initial degradation temperature of SL/GO was 240.86 °C, and the maximum weight loss occurred at 292.83 °C, with mass loss of 29.61%. The initial degradation temperature and maximum weight loss temperature of LCGH were observed at 318.73 °C and 347.20 °C, respectively, with mass loss of 31.51%. It was proved that the addition of SL and CS was helpful for enhancing the thermal stability of the LCGH [23,32], indicating an inner connecting structure of LCGH. In addition, the weight loss at 300–400 °C and 400–600 °C of LCGH was due to the pyrolysis of oxygen-containing functional groups in composite [33].

3.1.5. SEM

The morphology and structure of prepared composites were characterized by SEM in Figure 3. Liu et al. [15] showed that unmodified GO had a smooth surface and a flaky structure with wrinkled edges. The image of CS/GO composite showed plenty of small holes with thin sheets (Figure 3a), and the SL/GO composite showed ordered sheet structures with macroporous structures (Figure 3b). SL could insert into the GO layer and prevent the graphene sheets from severe agglomeration, and a macroporous structure was produced [23]. The layered structure and 3D reticular porous structure could be clearly observed in CS/SL/GO composite (LCGH) (Figure 3c). Yan et al. [23] showed that SL macromolecules were embedded in GO through noncovalent interactions, such as van der Waals force and π-π interaction. SL had many oxygen and sulfonic acid groups, and thus carried a negative charge, which dispersed the GO layer by strong electrostatic attraction. The hydroxyl and amine groups on CS made it possible to cross link GO and SL by hydrogen bonding and electrostatic force. Therefore, the cross-linking effect of CS and SL embedded in the GO layer can contribute to the construction of 3D porous materials conducive to pollutant diffusion and adsorption [34].
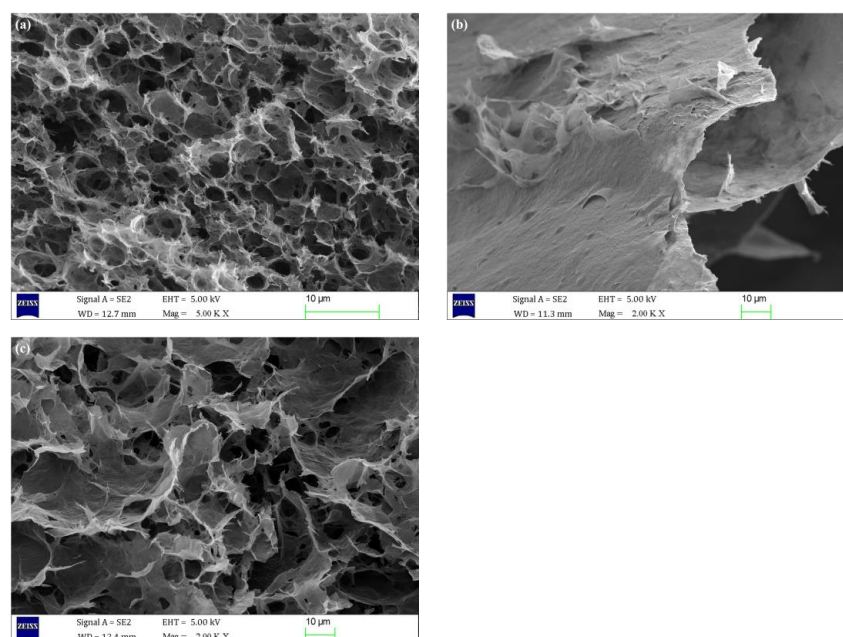

Figure 3. SEM images of samples (**a**) CS/GO = 1:10, (**b**) SL/GO = 1:1, (**c**) CS/SL/GO = 1:10:10.

3.2. Adsorption Experiments

3.2.1. The Effect of Mass Ratio of CS/SL/GO

The LCGH with CS/SL/GO mass ratios 1:5:10, 1:10:10, 1:10:5, and 1:5:5 and SL/GO 1:1 CS/GO 1:10 were applied to experimental investigation. As shown in Figure 4a, the content of CS, SL, and GO had a distinct influence on Cr(VI) removal. The addition of CS and SL in the composite obviously promoted the Cr(VI) removal. The LCGH composite with CS/SL/GO = 1:10:10 had better Cr(VI) removal than that of other composites. It was found that increasing the contents of SL and GO of the composite resulted in an increase in the Cr(VI) removal rate, suggesting that SL was beneficial for adsorption. However, increasing the content of CS decreased the Cr(VI) removal efficiency by LCGH composite. This was probably because the chitosan reacted with the GO and SL functional groups, which consumed more adsorption sites. In addition, too much CS could clog the three-dimensional porous structure, leading to the smaller LCGH adsorption area and greater loss of adsorption capacity [34]. Furthermore, the CS/SL/GO showed a higher removal efficiency than the composites of SL/GO and CS/GO, indicating an advantage of the LCGH composite. It could be concluded that composite with CS/SL/GO = 1:10:10 could be used as the best biosorbent for experiments.
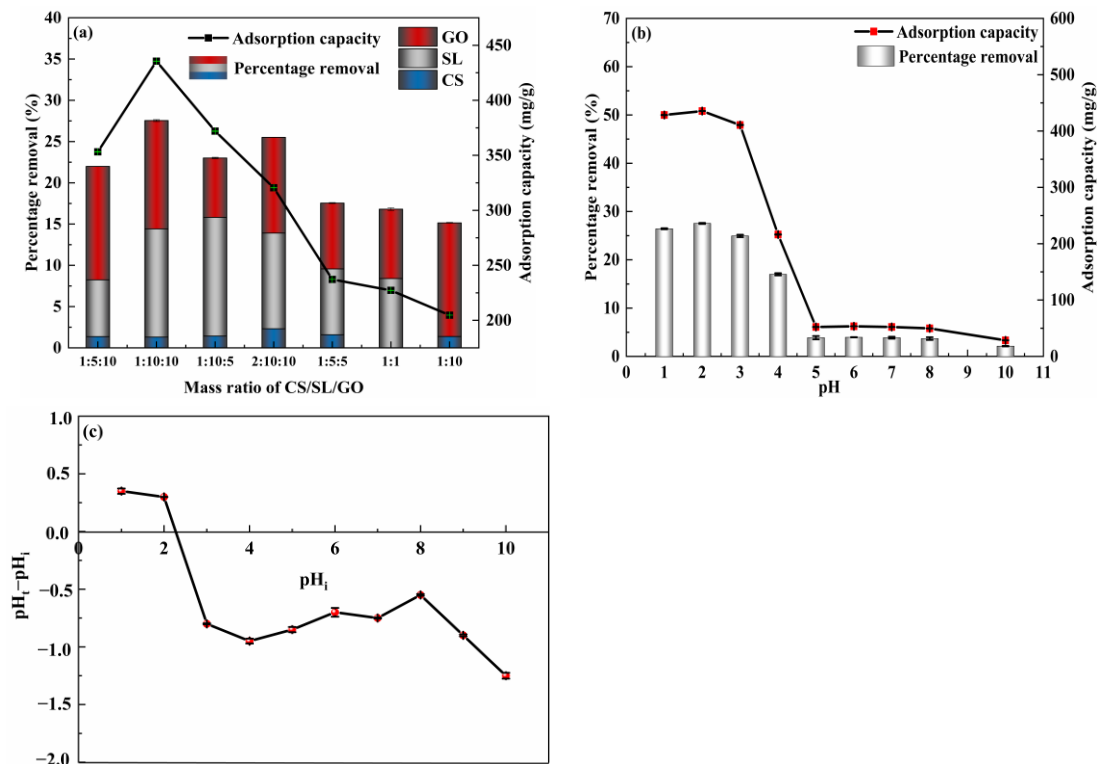

Figure 4. (**a**) Effect of mass ratio of CS:SL:GO on Cr(VI) adsorption (pH = 2.0), (**b**) Effect of pH on Cr(VI) adsorption by LCGH (CS/SL/GO = 1:10:10), (**c**) Isoelectric point analysis on the Cr(VI) adsorption by LCGH (CS/SL/GO = 1:10:10) (all the above conditions are C_0 = 50 mg/L, T = 298 K, t = 2 h).

3.2.2. Influence of pH

The pH has a certain effect on charge properties of adsorbed material surface, functional groups, and Cr(VI) valence states [35]. The adsorption properties improved as pH decreased (Figure 4b). The adsorption capacity was high under acid conditions (pH = 1.0–5.0) but lower under high pH conditions (pH = 5.0–10.0). This is because $HCrO_4^-$ and $Cr_2O_7^{2-}$ are the dominant species of Cr in acidic solutions [36], while CrO_4^{2-} is the dominant species under neutral and alkaline conditions (pH = 5.0–10.0). When the pH of the solution is less than 5.0, the surface of the LCGH could be protonated and tended to be positively charged.

The strong chemisorption and electrostatic attraction occurred between the chromium containing anions and the adsorbent of LCGH. The adsorption capacity of Cr(VI) was up to 435.58 mg/g. However, when pH was between 3.0 and 10.0, the adsorption performance deteriorated with the increasing pH. Under neutral and alkaline conditions, Cr(VI) mainly existed as $Cr_2O_7^{2-}$ and CrO_4^{2-}. Excessive OH^- and $Cr_2O_7^{2-}$/CrO_4^{2-} competitively adsorbed the active site of LCGH composites, resulting in less Cr(VI) adsorption capacity [37–39].

3.2.3. Isoelectric Point Analysis

The isoelectric point of LCGH was approximately 2.3 (Figure 4c), indicating that acidic group content on material surfaces was greater than that of basic groups [24]. First, the carboxyl, hydroxyl, sulfonic acid, and other functional groups on sample surface were protonated while the solution was in acidic condition (pH < 2.3), resulting in a positive charged surface of the sample which was conducive to adsorption. Second, the functional groups on sample surface were deprotonated while the pH > 2.3, resulting in negatively charged of the sample surface. Therefore, the OH^- competed with the chromium containing anions for sites of the adsorbent, which could reduce the adsorption efficiency [23]. This finding was in accordance with the result in pH analysis.

3.3. Theoretical Study of Cr(VI) Adsorption on LCGH
3.3.1. Adsorption Kinetics

In practical adsorption applications, contact time is an important influence due to the different types of solid–liquid interactions [40]. Due to more available active sites on LCGH, the adsorption capacity increased rapidly within 30 min (Figure 5). As the reaction progressed, the pores and sites on LCGH were gradually consumed, resulting in a trend of adsorption rate gradually slowing down before reaching equilibrium [23]. When Cr(VI) was 50 mg/L, LCGH (CS/SL/GO = 1:10:10) reached the adsorption equilibrium at T = 298 K for 3 h.

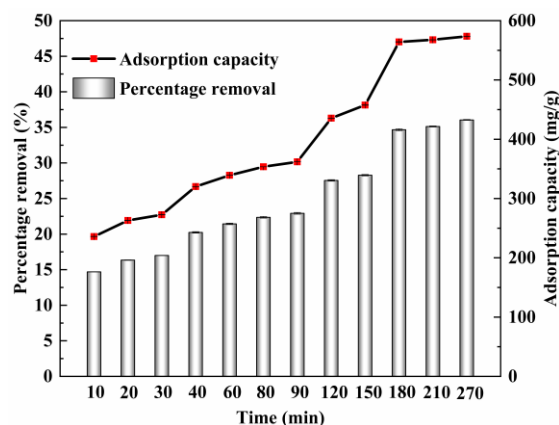**Figure 5.** Effect of reaction time on the Cr(VI) adsorption by LCGH (C_0 = 50 mg/L, T = 298 K, pH = 2.0, CS/SL/GO = 1:10:10).

To study the adsorption rate and control step, pseudo-first-order [41], pseudo-second-order [42], and intra-particle diffusion models were investigated as described below:

Pseudo-first-order:

$$In(q_e - q_t) = In q_e - K_1 t \tag{4}$$

Pseudo-second-order:

$$\frac{t}{q_t} = \frac{1}{K_2 \times q_e^2} + \frac{1}{q_e} \times t \tag{5}$$

where q_e and q_t are heavy metal ions adsorbed amounts (mg/g) at equilibrium and contact time t (min), respectively; k_1 (1/min) and k_2 (g/mg·min) are the rate constant.

The calculated q_e by pseudo first-order model was inconsistent with the experimental value (Table 1). R^2 was quite low (0.9645), indicating that the first-order model could not explain adsorption kinetics well. R^2 for the pseudo-second-order model was relatively high (0.9716), and the calculated q_e was very similar to the research result. As shown in Figure S1a, it suggested that the adsorption conformed to pseudo second-order. In addition, an intra-particle diffusion model suggested by Weber and Morris was adopted to learn the adsorption mechanism [43,44]:

Table 1. Adsorption kinetics fitting results of Cr(VI) on LCGH from three kinetic models.

Isotherm Model	Parameter	Value
Pseudo-first-order model	Q_e (mg/g)	129.12
	$K_1 \times 10^{-2}$ (min^{-1})	0.343
	R^2	0.9645
Pseudo-second-order model	Q_e (mg/g)	495.050
	h (mg/(g·mg))	22.6552
	$K_2 \times 10^{-4}$ [g·(mg·min)$^{-1}$]	0.9244
	R^2	0.9716
Intraparticle diffusion model	K_{int1} (mg/(g·min$^{0.5}$))	21.4413
	C_1	167.8161
	$R_1{}^2$	0.9692
	K_{int2} (mg/(g·min$^{0.5}$))	47.3354
	C_2	−89.3949
	$R_2{}^2$	0.9448
	K_{int3} (mg/(g·min$^{0.5}$))	3.1494
	C_3	521.9974
	$R_3{}^2$	0.9998

Intra-particle diffusion:

$$q_t = k_{int}t^{1/2} + C_i \tag{6}$$

where k_{int} (mol·g^{-1}·min$^{1/2}$) is the diffusion rate constant intra-particle and C_i is proportional to the boundary layer thickness.

If q_t versus $t^{1/2}$ shows a straight line, then adsorption includes intra-particle diffusion, and if this line goes through the origin, then intraparticle diffusion is the only rate-limiting step, calculating K_{int} from the slope and C_i from the intercept. Figure S1b showed the plot of q_t versus $t^{1/2}$ at initial Cr(VI) concentration. There were three parts suggesting the mass transfer on the LCGH (Table 1). In the first stage, the adsorption rate of LCGH was quiet fast, because Cr(VI) rapidly diffused to LCGH outer surface through bulk solution. The second stage was a gradual adsorption process, indicating that Cr(VI) diffused from the outer surface of the LCGH composite to the inner surface. With the gradual saturation of active sites in the inner pores, the contact surface between LCGH and Cr(VI) became smaller, and the adsorption rate became slower [45]. The third stage was the final equilibrium process: Cr(VI) moved very slowly, the adsorption sites were saturated, and finally equilibrium was reached. The finding showed that the rate constant order was $k_{int2} > k_{int1} > k_{int3}$ (Table 1), indicating that the adsorption rate of stage two was the highest. Because the LCGH composite had many active sites that could promote the Cr(VI) adsorption. As the process continued, the Cr(VI) adsorption finally reached equilibrium. The fact that the adsorption did not cross origin, indicated that the intra-particle diffusion model was not a key process for controlling the rate in the adsorption process.

3.3.2. Analysis of Adsorption Isotherms

The variations in adsorption capacity in different concentrations and a certain temperature range was discussed. The adsorption capacity improved with increased temperature and concentration in a certain range (CS/SL/GO = 1:10:10, pH = 2.0, t = 3 h) (Figure 6a). Especially at lower Cr (VI) concentration (<50 mg/L), it showed a sharp increase trend,

which was mainly due to strong electrostatic attraction. With the concentration increased, more Cr(VI) was adsorbed on LCGH until equilibrium was reached (50 mg/L) [46]. The maximum Cr(VI) adsorption capacity could reach 564.2 mg/g at T = 298 K in the range of the experimental concentration.
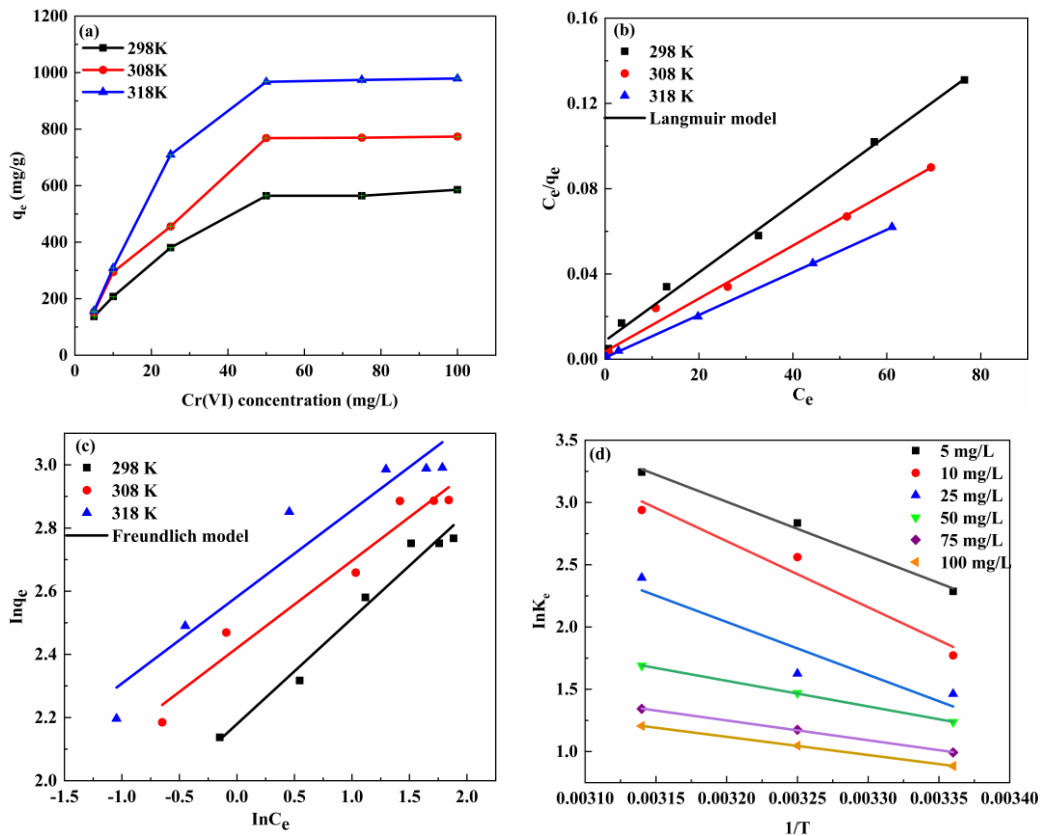

Figure 6. (**a**) Effect of initial concentration on the Cr(VI) adsorption by LCGH (CS/SL/GO = 1:10:10, pH = 2.0, t = 3 h), (**b**) Langmuir isotherm model, (**c**) Freundlich isotherm model (CS/SL/GO = 1:10:10, pH = 2.0, t = 3 h), (**d**) adsorption thermodynamics LCGH on the Cr(VI) adsorption (C_0 = 50 mg/L, T = 298 K, t = 3 h, pH = 2.0, CS/SL/GO = 1:10:10).

The Langmuir and Freundlich models [47] were to further study the adsorption isotherms, and linear equations were as follows:

Langmuir:

$$\frac{C_e}{q_e} = \frac{1}{q_m \cdot K_L} + \frac{C_e}{q_m} \tag{7}$$

$$R_L = \frac{1}{1 + K_L \cdot C_0} \tag{8}$$

where q_e is Cr(VI) ion adsorbed amount on the adsorbent (mg/g), C_e is the equilibrium Cr(VI) concentration (mg/L). q_m stands for saturated adsorption capacity. K_L (L/mg) is the Langmuir isotherm adsorption equation constant. The R_L ($1 \geq R_L \geq 0$) means that the adsorption is easy to occur [48].

Freundlich:

$$In q_e = In K_F + \frac{1}{n} In C_e \tag{9}$$

where K_F (L/g) is the Freundlich constant representing adsorption capacity and *n* is the heterogeneous factor of adsorption strength.

The fitting results of adsorption equilibrium with the Langmuir and Freundlich models were shown in Figure 6b,c and Table S1. The Cr(VI) adsorption on LCGH could be well described with the Langmuir adsorption model (R^2 = 0.9951) and with the saturated

adsorption capacity (621.12 mg/g), which followed the study result (564.2 mg/g) (Figure 6b and Table S1). Thus, we may infer that Cr(VI) adsorption on LCGH was mainly monolayer. In addition, R_L was between 0~1 (Table S2), which was favorable for adsorption. As the Cr(VI) concentration increased, R_L decreased, indicating that high Cr(VI) concentrations facilitated adsorption, which followed the experiments with different concentrations described above. For the Freundlich model, the low R^2 (0.9743) suggested that the adsorption was inconsistent with the model (Figure 6c). However, $n > 1$ illustrated that the adsorption was advantageous under high strength.

3.3.3. Adsorption Thermodynamics

To further learn the mechanism of LCGH effect on Cr(VI) structure, according to Cr(VI) equilibrium concentration (C_e) and adsorption capacity (Q_e) on LCGH, the adsorption equilibrium constants t K_e at different temperatures were obtained at 298, 308, and 318 K. According to the Van't Hoff equation, the thermodynamic parameters of Cr(VI) adsorption were calculated by plotting InK_e vs. $1/T$ [48] (Figure 6d):

$$\Delta G = -RTInK_e \tag{10}$$

$$K_e = \frac{Q_e}{C_e} \tag{11}$$

$$nK_e = \frac{\Delta S^0}{R} - \frac{\Delta H^0}{RT} \tag{12}$$

where T and R are the thermodynamic temperature and gas constant, respectively. ΔG, ΔS^0, and ΔH^0 are the change in Gibbs free energy, entropy and enthalpy, respectively. The results are shown in Table 2.

Table 2. Adsorption thermodynamics fitting results for Cr(VI) on LCGH.

Concentration (mg/L)	Temp.	K_e	ΔG (kJ/mol)	ΔH (kJ/mol)	ΔS (kJ/(mol·K))	R^2
5	298 K	193.4111	−5.8550	36.1735	0.1407	0.9929
	308 K	683.8367	−7.4952			
	318 K	1752.6599	−8.8455			
10	298 K	59.1725	−4.5379	44.1209	0.1635	0.9603
	308 K	364.3415	−6.7722			
	318 K	870.2609	−8.0164			
25	298 K	29.0520	−3.7468	35.2438	0.1297	0.8762
	308 K	42.2562	−4.2986			
	318 K	248.7869	−6.5334			
50	298 K	17.2718	−3.1685	17.1003	0.06776	0.9998
	308 K	29.4458	−3.8839			
	318 K	48.9530	−4.6080			
75	298 K	9.8444	−2.5433	13.2117	0.05267	0.9995
	308 K	14.9613	−3.1064			
	318 K	22.0170	−3.6617			
100	298 K	7.6527	−2.2632	12.1384	0.04814	0.9999
	308 K	11.1510	−2.7689			
	318 K	16.0341	−3.2861			

The negative value of ΔG at different concentrations and temperatures showed that Cr(VI) adsorption on LCGH was spontaneous, and the higher the temperature, the more favorable for adsorption to proceed, which conformed to results obtained by the isothermal model [49]. In general, the absolute magnitude of standard free energy change (ΔG^0) for physical adsorption is between 0 and 20 kJ·mol^{-1} [50]. The Cr(VI) adsorption on LCGH ($|\Delta G|$) at the experimental temperature range (from 298 and 318 K) was less than 20 kJ·mol^{-1}, showing that the adsorption was physical. The interaction was dominated by electrostatic attraction with positive entropy and small negative enthalpy

($\Delta H > 0$, $\Delta S > 0$) [51]. The transfer of Cr(VI) from solution to LCGH was entropic favorable ($\Delta S > 0$) and enthalpy unfavorable ($\Delta H > 0$) (Table 2), indicating that the adsorption process was entropy-driven through hydrophobic interactions. Even though the entropy change was reduced, the adsorption capacity increased with increasing surfactant loading (characterized by increased $|\Delta G|$), which was caused by the decrease in the unfavorable enthalpy change. In conclusion, the LCGH composite had high adsorption capacity for Cr(VI) compared with other materials (Table 3).

Table 3. Adsorption properties of Cr(VI) by lignosulfonate-modified and graphene-based adsorbents in the literatures.

Adsorbent	Pollutants	Adsorption Capacity(mg/g)	Reference
MLS	Cr(VI)	57.1	[11]
SLACM	Cr(VI)	227.7	[13]
LS-g-P (AM-co-DAC)	Cr(VI)	58.86	[52]
N-LEGO	Cr(VI)	416.97	[53]
Lignosulfonate-modified graphene hydrogel (LCGH)	Cr(VI)	564.2	This work

3.4. Adsorption Mechanism

As shown in Figure 7, the mechanism of efficient adsorption was due to the interaction between Cr(VI) ion and oxygen containing groups such as phenol and carboxyl groups on LCGH composite [10]. FT-IR spectra of Cr(VI)-loaded LCGH (LCGH-Cr) demonstrated a slight shift in the spectral position and a significant change in intensity (Figure 7). The peaks at 3255 and 1650 cm^{-1} in LCGH appeared at 3252 and 1660 cm^{-1} in LCGH-Cr, which corresponded to O–H and C–C stretching, respectively, implying that hydrogen bond and π-π interaction existed in Cr(VI) adsorption [23]. The bands at 1760 and 1015 cm^{-1} of LCGH belonged to C=O and S=O and moved to 1753 and 1009 cm^{-1}, respectively, implying that the electrostatic interaction between sulfonic acid and carboxyl groups was the main part of Cr(VI) adsorption by LCGH [9]. In addition, the N–H and C–N at 1153 and 1380 cm^{-1} moved to 1149 and 1376 cm^{-1}, respectively, implying that there were hydrogen bonds between amino and hydroxyl groups of LCGH. In addition, new peaks appeared at 916 and 563 cm^{-1} corresponded to CrO_4^{2-} and formation of $Cr(OH)_3$ in LCGH-Cr, respectively [54].
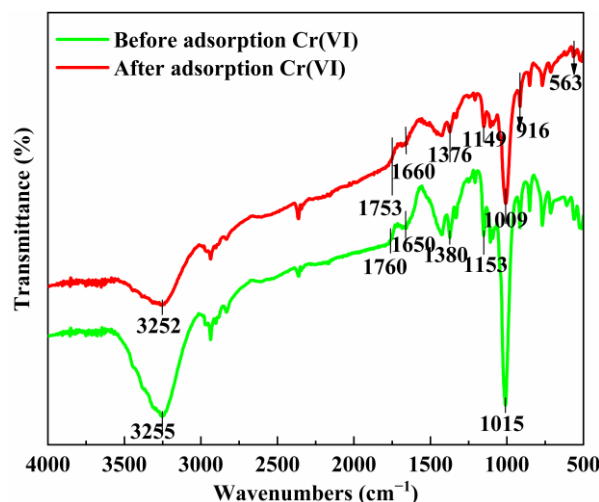

Figure 7. FT-IR spectra of the adsorbent.

In conclusion, the adsorption mechanism of Cr(VI) by LCGH could be summarized as follows: (1) electrostatic attraction, under the experimental condition (pH = 2), the

carboxyl group, sulfonic acid group, and amino group on the surface of LCGH underwent protonation and interacted with negatively charged Cr(VI) in solution, and this adsorption process was effective; (2) according to the results of kinetics, isothermal process, and XPS analysis, the adsorption process was a physical–chemical composite adsorption of monolayer on uniform surface. Surface adsorption was mainly chemical adsorption with chemical bonds such as oxygen-containing functional groups and amino groups with Cr(VI). Therefore, it can be deduced that chemisorption is the main process of adsorption.

3.5. Influence of Co-Existing Heavy Metal Ions

The Cr(VI) adsorption experiment in Cu(II)/Cr(VI) and Zn(II)/Cr(VI) binary systems and Cu(II)+Zn(II)/Cr(VI) ternary system by LCGH was conducted to explore the properties of the biosorbent in the actual polluted wastewater. As shown in Figure 8a, the 'blank' is the adsorption of LCGH only for Cr(VI), and the influence of binary and ternary systems were explored of Cu(II)/Cr(VI), Zn(II)/Cr(VI), and Cu(II) + Zn(II) (1:1)/Cr(VI) under the conditions of mass concentration ratios of 1:1, 2:1, 3:1, 4:1 on Cr(VI) adsorption performance. For the Zn(II)/Cr(VI) binary system, the Cr(VI) adsorption capacity dropped from 564.2 mg/g to 353.5 mg/g, and the removal efficiency decreased from 34.67% to 26.16%, respectively. For Cu(II)/Cr(VI) binary system, the Cr(VI) adsorption capacity decreased from 564.2 mg/g to 414.7 mg/g, and the removal efficiency decreased from 34.67% to 30.69%, respectively. For the Zn(II)+Cu(II)/Cr(VI) ternary system, the Cr(VI) adsorption capacity decreased from 564.2 mg/g to 394.7 mg/g, and the removal efficiency decreased from 34.67% to 29.21%, respectively. The adsorption capacity and removal efficiency of Cr(VI) by LCGH decreased with the increase in coexisting ion concentration, and the order of the inhibition degree for Cr(VI) adsorption was (Zn(II) > Cu(II)+Zn(II) > Cu(II)). Obviously, the existence of Zn(II) and Cu(II) interfered with the Cr(VI) adsorption by LCGH because Zn(II) and Cu(II) competed with Cr(VI) for the active adsorption site on LCGH and hinder Cr(VI) diffusion, which caused the decrease in Cr(VI) adsorption capacity [55,56]. In addition, the metal cations can also bind to chromium anions, thus reducing the Cr(VI) adsorption capacity. This discovery was similar to the results of Dong et al., who found that the existence of Cu(II) reduced the Cr(VI) adsorption capacity by the cetyl trimethyl ammonium bromide (CTAB) modified Auricularia auricula spent substrate (AASS) material. Although the modified material could adsorb chromium anions and repel other coexisting metal cations when it was positively charged under experimental conditions, the metal cations could combine with chromium anions, thus reducing the Cr(VI) removal efficiency [57]. Moreover, the reason for the difference in inhibition degree between Zn(II) and Cu(II) was that the hydration radius of Cu(II) was smaller than Zn(II), and the smaller hydration radius was easier to diffuse to the surface of the adsorbent, thus LCGH had a stronger affinity for Cu(II) [58,59]. Therefore, it could be inferred that LCGH had no selectivity in adsorbing heavy metal ions and could be used to remove various ionic pollutants in wastewater.
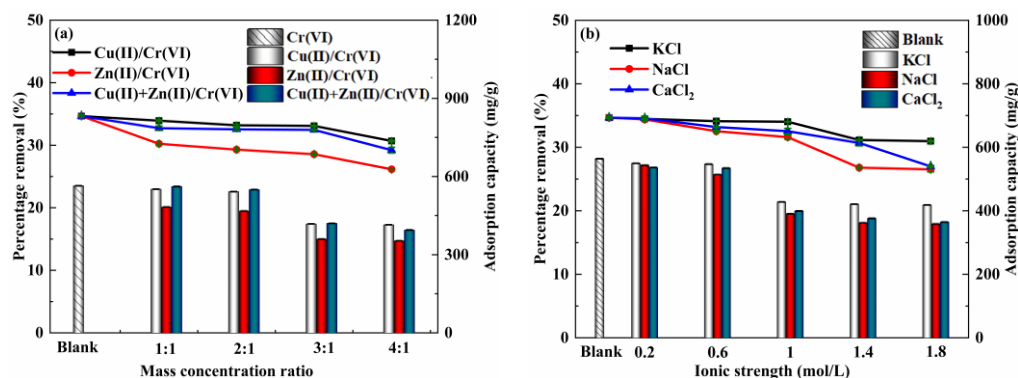

Figure 8. Effect of (**a**) coexisting ion and (**b**) ionic strength for LCGH on the Cr(VI) adsorption (C_0 = 50 mg/L, T = 298 K, t = 3 h, pH = 2.0, CS/SL/GO = 1:10:10).

3.6. Influence of Inorganic Ions

As shown in Figure 8b, compared with Cr(VI) adsorption without inorganic ion addition (blank), the addition of coexisting inorganic ions such as Ca^{2+}, K^+, and Na^+ in Cr(VI) solution (without Cu(II) and Zn(II) addition) was to investigate the Cr(VI) adsorption performance on LCGH in practical application. As the concentration of ionic strength increased (0–1.8 mol/L), the Cr(VI) adsorption properties on LCGH constantly decreased, indicating that these three ions interfered with the Cr(VI) adsorption on LCGH. It could be inferred that there was a competitive adsorption between these three ions and Cr(VI) on LCGH biosorbent, and the interference degree for Cr(VI) adsorption was $Na^+ > Ca^{2+} > K^+$. That means the existence of Na^+ could decrease more of the Cr(VI) adsorption by LCGH than the presence of Ca^{2+} and K^+ in the wastewater. The reason may be that the increase in ionic strength reduced the Cr(VI) activity, which hindered the Cr(VI) diffused from solution to LCGH surface, resulting in the decrease of heavy metals onto the biosorbent [17,60].

3.7. Practical Application and Reusability Study

In order to verify the practical application of LCGH material for Cr(VI) removal, simulated wastewater was used to verify Cr(VI) adsorption performance by LCGH. The composition of simulated electroplating wastewater could be seen in Table 4 [61]. The adsorption capacity and efficiency of LCGH for Cr(VI) removal were 207.32 mg/g and 19.70%, respectively (Figure 9a). Compared with the Cr(VI) adsorption experiment in pure water (564.22 mg/g, 34.67%), the adsorption performance of LCGH for Cr (VI) decreased, but the adsorption capacity of LCGH was still higher than other materials. The reason for this phenomenon was that various metal ions in the simulated wastewater competed with Cr(VI) for the adsorption site on LCGH materials, and inorganic salt ions also inhibited the Cr(VI) adsorption on LCGH. Even though the simulated actual wastewater environment was complex, LCGH still exhibited a good performance for Cr(VI) adsorption.

Table 4. The substance content in simulated electroplating wastewater.

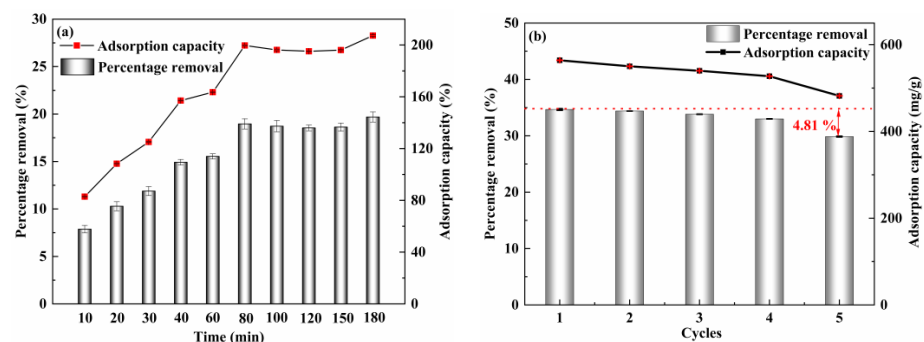| Composition	Simulated Electroplating Wastewater (mg/L)
Cr(VI)	100.0
Cu^{2+}	12.4
Ni^{2+}	5.3
Fe^{3+}	5.5
Al^{3+}	3.4
Zn^{2+}	6.7
Ca^{2+}	15.0
Cl^-	53.9
SO_4^{2-}	126.5
COD	-

Figure 9. (**a**) Adsorption properties of Cr (VI) removal by LCGH from simulated electroplating wastewater (T = 298 K, pH = 2.0, CS/SL/GO = 1:10:10), (**b**) effect of recycling LCGH on the Cr(VI) adsorption (C_0 = 50 mg/L, T = 298 K, t = 3 h, pH = 2.0, CS/SL/GO = 1:10:10).

The experimental conditions for exploring best adsorption performance were CS/SL/GO = 1:10:10, pH = 2, reaction time 3 h, and T = 298 K (Figure 9b). After five cycles of regeneration, the Cr(VI) removal rate was only reduced by 4.81% compared with the first cycle, and the adsorption capacity was reduced from 564.2 mg/g in the first time to 482.1 mg/g in the fifth time with the high adsorption capacity of 85.4%. Although the quality of LCGH composite was lost to a certain extent as the adsorption cycles increased, the final cycle performance test showed that LCGH possessed excellent regeneration performance. These results indicated that LCGH had a promising application prospect in removing Cr(VI) from wastewater.

4. Conclusions

The prepared LCGH had a cross-linked three-dimensional porous network, which made Cr(VI) easily diffuse to the surface of the LCGH composite. An adsorption experiment indicated that the LCGH could achieve strong adsorption capacity (564.2 mg/g) for Cr(VI), which was related to the 3D porous structure and functional groups of LCGH. The main adsorption mechanisms were hydrogen bond, π-π interaction, and electrostatic attraction. In addition, the LCGH showed good cyclic regeneration in practical application, and its adsorption capacity could still be retained up to 85.4% after five cycles. In summary, the LCGH has great application potential in Cr(VI) removal from wastewater.

Supplementary Materials: The following supporting information can be downloaded at: https://www.mdpi.com/article/10.3390/w14223684/s1, Figure S1: (a) pseudo-first-order model and pseudo-second-order kinetic model, (b) Intraparticle diffusion model; Table S1: Langmuir and Freundlich isotherm models fitting parameters for Cr(VI) adsorption on LCGH at the range of temperature of 298 K–318 K; Table S2: R$_L$ values based on the Langmuir equation.

Author Contributions: Methodology and data curation, C.H.; writing-original draft preparation, C.H. and X.L.; visualization, T.W.; conceptualization, X.S.; formal analysis, X.L. and L.B.; funding acquisition, resources, and supervision, Y.S. All authors have read and agreed to the published version of the manuscript.

Institutional Review Board Statement: Not applicable.

Informed Consent Statement: Not applicable.

Data Availability Statement: Not applicable.

Conflicts of Interest: The authors declare no conflict of interest.

References

1. Xu, H.; Gao, M.; Hu, X.; Chen, Y.; Li, Y.; Xu, X.; Zhang, R.; Yang, X.; Tang, C.; Hu, X. A novel preparation of S-NZVI and its high efficient removal of Cr(VI) in aqueous solution. *J. Hazard. Mater.* **2021**, *416*, 125924. [CrossRef] [PubMed]
2. Zhang, Y.H.; Xu, X.M.; Yue, C.L.; Song, L.; Lv, Y.Z.; Liu, F.Q.; Li, A.M. Insight into the efficient co-removal of Cr(VI) and Cr(III) by positively charged UiO-66-NH2 decorated ultrafiltration membrane. *Chem. Eng. J.* **2021**, *404*, 126546–126555. [CrossRef]
3. Xie, Y.Q.; Lin, J.; Liang, J.; Li, M.H.; Fu, Y.W.; Wang, H.T.; Tu, S.; Li, J. Hypercrosslinked mesoporous poly(ionic liquid)s with high density of ion pairs: Efficient adsorbents for Cr(VI) removal via ion-exchange. Chem. *Eng. J.* **2019**, *378*, 122107–122116. [CrossRef]
4. Yang, X.D.; Wan, Y.S.; Zheng, Y.L.; He, F.; Yu, Z.B.; Huang, J.; Wang, H.L.; Ok, Y.S.; Jiang, Y.S.; Gao, B. Surface functional groups of carbon-based adsorbents and their roles in the removal of heavy metals from aqueous solutions: A critical review. *Chem. Eng. J.* **2019**, *366*, 608–621. [CrossRef] [PubMed]
5. Chen, F.J.; Yu, W.C.; Qie, Y.; Zhao, L.X.; Zhang, H.; Guo, L.H. Enhanced photocatalytic removal of hexavalent chromium through localized electrons in polydopamine-modified TiO$_2$ under visible irradiation. *Chem. Eng. J.* **2019**, *373*, 58–67. [CrossRef]
6. Sun, Y.C.; Liu, X.N.; Lv, X.T.; Wang, T.T.; Xue, B.L. Synthesis of novel lignosulfonate-modified graphene hydrogel for ultrahigh adsorption capacity of Cr(VI) from wastewater. *J. Clean. Prod.* **2021**, *295*, 126406–126418. [CrossRef]
7. Sun, X.T.; Yang, L.R.; Li, Q.; Liu, Z.N.; Dong, T.T.; Liu, H.Z. Polyethylenimine-functionalized poly(vinyl alcohol) magnetic microspheres as a novel adsorbent for rapid removal of Cr(VI) from aqueous solution. *Chem. Eng. J.* **2015**, *262*, 101–108. [CrossRef]
8. Al-Othman, Z.A.; Ali, R.; Naushad, M. Hexavalent chromium removal from aqueous medium by activated carbon prepared from peanut shell: Adsorption kinetics, equilibrium and thermodynamic studies. *Chem. Eng. J.* **2012**, *184*, 238–247. [CrossRef]

9.　Zhou, H.F.; Shi, X.X.; Wu, W.D.; An, X.X.; Tian, Y.Y.; Qiao, Y.Y. Facile preparation of lignosulfonate/N-methylaniline composite and its application in efficient removal of Cr(VI) from aqueous solutions. *Int. J. Biol. Macromol.* **2020**, *154*, 1194–1204. [CrossRef]

10.　Li, F.F.; Wang, X.L.; Yuan, T.Q.; Sun, R.C. Lignosulfonate-modified graphene hydrogel with ultrahigh adsorption capacity for Pb(II) removal. *J. Mater. Chem. A* **2016**, *4*, 11888–11896. [CrossRef]

11.　Geng, J.; Gu, F.; Chang, J.M. Fabrication of magnetic lignosulfonate using ultrasonic-assisted in situ synthesis for efficient removal of Cr(VI) and Rhodamine B from wastewater. *J. Hazard. Mater.* **2019**, *375*, 174–181. [CrossRef] [PubMed]

12.　Myglovets, M.; Poddubnaya, O.I.; Sevastyanova, O.; Lindström, M.E.; Gawdzik, B.; Sobiesiak, M.; Tsyba, M.M.; Sapsay, V.I.; Klymchuk, D.O.; Puziy, A.M. Preparation of carbon adsorbents from lignosulfonate by phosphoric acid activation for the adsorption of metal ions. *Carbon* **2014**, *80*, 771–783. [CrossRef]

13.　Yang, K.Y.; Xing, J.C.; Xu, P.P.; Chang, J.M.; Zhang, Q.F.; Usman, K.M. Activated carbon microsphere from sodium lignosulfonate for Cr(VI) adsorption evaluation in wastewater treatment. *Polymers* **2020**, *12*, 236. [CrossRef]

14.　Sun, Z.Q.; Liao, T.; Li, W.X.; Qiao, Y.X.; Ostrikov, K. Beyond seashells: Bioinspired 2D photonic and photoelectronic devices. *Adv. Funct. Mater.* **2019**, *29*, 1901460–1901484. [CrossRef]

15.　Liu, Y.; Xu, L.; Liu, J.S.; Liu, X.Y.; Chen, C.H.; Li, G.Y.; Meng, Y.F. Graphene oxides cross-linked with hyperbranched polyethylen-imines: Preparation, characterization and their potential as recyclable and highly efficient adsorption materials for lead(II) ions. *Chem. Eng. J.* **2016**, *285*, 698–708. [CrossRef]

16.　Luo, J.Q.; Fan, C.J.; Xiao, Z.; Sun, T.S.; Zhou, X.D. Novel graphene oxide/carboxymethyl chitosan aerogels via vacuum-assisted self-assembly for heavy metal adsorption capacity. *Colloid. Surface. A.* **2019**, *578*, 123584–123594. [CrossRef]

17.　Bao, S.Y.; Yang, W.W.; Wang, Y.J.; Yu, Y.S.; Sun, Y.Y.; Li, K.F. PEI grafted amino-functionalized graphene oxide nanosheets for ultrafast and high selectivity removal of Cr(VI) from aqueous solutions by adsorption combined with reduction: Behaviors and mechanisms. *Chem. Eng. J.* **2020**, *399*, 125762–125772. [CrossRef]

18.　Lei, Y.; Chen, F.; Luo, Y.; Zhang, L. Synthesis of three-dimensional graphene oxide foam for the removal of heavy metal ions. *Chem. Phys. Lett.* **2014**, *593*, 122–127. [CrossRef]

19.　Sakr, A.K.; Abdel Aal, M.M.; Abd El-Rahem, K.A.; Allam, E.M.; Abdel Dayem, S.M.; Elshehy, E.A.; Hanfi, M.Y.; Alqahtani, M.S.; Cheira, M.F. Characteristic Aspects of Uranium(VI) Adsorption Utilizing Nano-Silica/Chitosan from Wastewater Solution. *Nanomaterials* **2022**, *12*, 3866. [CrossRef]

20.　Wang, F.; Gao, J.; Jia, L.; Wang, S.; Ning, P. Green synthesis of a novel functionalized chitosan adsorbent for Cu(II) adsorption from aqueous solution. *Environ. Sci. Pollut. Res. Int.* **2022**, *29*, 989–998. [CrossRef]

21.　Kuczajowska-Zadrożna, M.; Filipkowska, U.; Jóźwiak, T. Adsorption of Cu (II) and Cd (II) from aqueous solutions by chitosan immobilized in alginate beads. *J. Environ. Chem. Eng.* **2020**, *8*, 103878. [CrossRef]

22.　Pincus, L.N.; Petrović, P.V.; Gonzalez, I.S.; Stavitski, E.; Fishman, Z.S.; Rudel, H.E.; Anastas, P.T.; Zimmerman, J.B. Selective adsorption of arsenic over phosphate by transition metal cross-linked chitosan. *Chem. Eng. J.* **2021**, *412*, 128582–128592. [CrossRef]

23.　Yan, M.F.; Huang, W.X.; Li, Z.L. Chitosan cross-linked graphene oxide/lignosulfonate composite aerogel for enhanced adsorption of methylene blue in water. *Int. J. Biol. Macromol.* **2019**, *136*, 927–935. [CrossRef] [PubMed]

24.　Li, Z.L.; Ge, Y.Y.; Wan, L. Fabrication of a green porous lignin-based sphere for the removal of lead ions from aqueous media. *J. Hazard. Mater.* **2015**, *285*, 77–83. [CrossRef]

25.　Musico, Y.L.F.; Santos, C.M.; Dalida, M.L.P.; Rodrigues, D.F. Improved removal of lead(II) from water using a polymer-based graphene oxide nanocomposite. *J. Mater. Chem. A* **2013**, *1*, 3789–3796. [CrossRef]

26.　Yao, Q.X.; Xie, J.J.; Liu, J.X.; Kang, H.M.; Liu, Y. Adsorption of lead ions using a modified lignin hydrogel. *J. Polym. Res.* **2014**, *21*, 465–480. [CrossRef]

27.　Dragan, E.S.; Cocarta, A.I.; Dinu, M.V. Facile fabrication of chitosan/poly(vinyl amine) composite beads with enhanced sorption of Cu^{2+}. Equilibrium, kinetics, and thermodynamics. *Chem. Eng. J.* **2014**, *255*, 659–669. [CrossRef]

28.　Choi, J.S.; Lingamdinne, L.P.; Yang, J.K.; Chang, Y.Y.; Koduru, J.R. Fabrication of chitosan/graphene oxide-gadolinium nanorods as a novel nanocomposite for arsenic removal from aqueous solutions. *J. Mol. Liq.* **2020**, *320*, 114410–114420. [CrossRef]

29.　Liu, S.Y.; Lai, C.; Li, B.S.; Zhang, C.; Zhang, M.M.; Huang, D.L.; Qin, L.; Yi, H.; Liu, X.G.; Huang, F.L.; et al. Role of radical and non-radical pathway in activating persulfate for degradation of p-nitrophenol by sulfur-doped ordered mesoporous carbon. *Chem. Eng. J.* **2020**, *384*, 123304–123313. [CrossRef]

30.　Kwak, H.W.; Shin, M.; Yun, H.; Lee, K.H. Preparation of silk sericin/lignin blend beads for the removal of hexavalent chromium ions. *Int. J. Mol. Sci.* **2016**, *17*, 1466. [CrossRef]

31.　Han, D.L.; Yan, L.F.; Chen, W.F. Preparation of chitosan/graphene oxide composite film with enhanced mechanical strength in the wet state. *Carbohydr. Polym.* **2011**, *83*, 653–658. [CrossRef]

32.　Chen, H.; Liu, T.L.; Meng, Y.; Cheng, Y.; Lu, J.; Wang, H.S. Novel graphene oxide/aminated lignin aerogels for enhanced adsorption of malachite green in wastewater. *Colloid. Surface. A* **2020**, *603*, 125281–125289. [CrossRef]

33.　Zhang, J.P.; Wang, Q.; Wang, A.Q. Synthesis and characterization of chitosan-g-poly(acrylic acid)/attapulgite superabsorbent composites. *Carbohydr. Polym.* **2007**, *68*, 367–374. [CrossRef]

34.　Wu, Z.J.; Shan, X.Y.; Li, Z.L. Preparation of a porous graphene oxide/alkali lignin aerogel composite and its adsorption properties for methylene blue. *Int. J. Biol. Macromol.* **2020**, *143*, 325–333. [CrossRef] [PubMed]

35.　Wang, Z.; Chen, G.H.; Wang, X.R.; Li, S.P.; Liu, Y.; Yang, G.H. Removal of hexavalent chromium by bentonite supported organosolv lignin-stabilized zero-valent iron nanoparticles from wastewater. *J. Clean. Prod.* **2020**, *267*, 122009–122019. [CrossRef]

36. Gu, H.B.; Rapole, S.B.; Huang, Y.D.; Cao, D.M.; Luo, Z.P.; Wei, S.Y.; Guo, Z.H. Synergistic interactions between multi-walled carbon nanotubes and toxic hexavalent chromium. *J. Mater. Chem. A* **2013**, *1*, 2011–2021. [CrossRef]

37. Kwak, H.W.; Kim, M.K.; Lee, J.Y.; Yun, H.; Kim, M.H.; Park, Y.H.; Lee, K.H. Preparation of bead-type biosorbent from water-soluble Spirulina platensis extracts for chromium (VI) removal. *Algal. Res.* **2015**, *7*, 92–99. [CrossRef]

38. Zhao, J.Q.; Lu, C.H.; He, X.; Zhang, X.F.; Zhang, W.; Zhang, X.M. Polyethylenimine-grafted cellulose nanofibril aerogels as versatile vehicles for drug delivery. *ACS Appl. Mater. Interfaces* **2015**, *7*, 2607–2615. [CrossRef]

39. Fernandez, P.M.; Vinarta, S.C.; Bernal, A.R.; Cruz, E.L.; Figueroa, L.I.C. Bioremediation strategies for chromium removal: Current research, scale-up approach and future perspectives. *Chemosphere* **2018**, *208*, 139–148. [CrossRef]

40. Ahmad, A.A.; Hameed, B.H.; Aziz, N. Adsorption of direct dye on palm ash: Kinetic and equilibrium modeling. *J. Hazard. Mater.* **2007**, *141*, 70–76. [CrossRef]

41. Tseng, R.L.; Wu, F.C.; Juang, R.S. Characteristics and applications of the Lagergren's first-order equation for adsorption kinetics. *J. Taiwan Inst. Chem. E.* **2010**, *41*, 661–669. [CrossRef]

42. Ho, Y.S.; McKay, G. Pseudo-second order model for sorption processes. *Process. Biochem.* **1999**, *34*, 451–465. [CrossRef]

43. Jahangiri, M.; Kiani, F.; Tahermansouri, H.; Rajabalinezhad, A. The removal of lead ions from aqueous solutions by modified multi-walled carbon nanotubes with 1-isatin-3-thiosemicarbazone. *J. Mol. Liq.* **2015**, *212*, 219–226. [CrossRef]

44. Ho, Y.S.; McKay, G. Comparative sorption kinetic studies of dye and aromatic compounds onto fly ash. *J. Environ. Sci. Health A* **1999**, *34*, 1179–1204. [CrossRef]

45. Rusmirovic, J.D.; Obradovic, N.; Perendija, J.; Umicevic, A.; Kapidzic, A.; Vlahovic, B.; Pavlovic, V.; Marinkovic, A.D.; Pavlovic, V.B. Controllable synthesis of Fe3O4-wollastonite adsorbents for efficient heavy metal ions/oxyanions removal. *Environ. Sci. Pollut. Res.* **2019**, *26*, 12379–12398. [CrossRef]

46. Pehlivan, E.; Altun, T. The study of various parameters affecting the ion exchange of Cu^{2+}, Zn^{2+}, Ni^{2+}, Cd^{2+}, and Pb^{2+} from aqueous solution on Dowex 50 W synthetic resin. *J. Hazard. Mater.* **2006**, *134*, 149–156. [CrossRef]

47. Langmuir, I. Adsorption of gases on glass, mica and platinum. *J. Am. Chem. Soc.* **1918**, *40*, 1361–1403. [CrossRef]

48. Sarin, V.; Singh, T.S.; Pant, K.K. Thermodynamic and breakthrough column studies for the selective sorption of chromium from industrial effluent on activated eucalyptus bark. *Bioresour. Technol.* **2006**, *97*, 1986–1993. [CrossRef]

49. Fu, J.W.; Chen, Z.H.; Wang, M.H.; Liu, S.J.; Zhang, J.H.; Zhang, J.A.; Han, R.P.; Xu, Q. Adsorption of methylene blue by a high-efficiency adsorbent (polydopamine microspheres): Kinetics, isotherm, thermodynamics and mechanism analysis. *Chem. Eng. J.* **2015**, *259*, 53–61. [CrossRef]

50. Gereli, G.; Seki, Y.; Murat Kusoglu, I.; Yurdakoc, K. Equilibrium and kinetics for the sorption of promethazine hydrochloride onto K10 montmorillonite. *J. Colloid Interface Sci.* **2006**, *299*, 155–162. [CrossRef]

51. Ross, P.D.; Subramanian, S. Thermodynamics of protein association reactions: Forces contributing to stability. *Biochemistry* **1981**, *20*, 3096–3102. [CrossRef] [PubMed]

52. Wei, S.X.; Chen, W.; Li, Z.L.; Liu, Z.Z.; Xu, A. Synthesis of cationic biomass lignosulfonate hydrogel for the efficient adsorption of Cr(VI) in wastewater with low pH. *Environ. Technol.* **2021**, 1–14, *ahead-of-print*. [CrossRef]

53. Geng, J.J.; Liang, Q.W.; Yu, W.Y.; Chen, W.; Lu, G.N.; Luo, H.J. Enhanced removal of Cr(VI) from aqueous solutions by polymer-mediated nitrogen-rich reduced graphene oxide. *J. Hazard. Mater.* **2022**, *436*, 129184. [PubMed]

54. Ko, Y.G.; Choi, U.S.; Kim, T.Y.; Ahn, D.J.; Chun, Y.J. FT-IR and isotherm study on anion adsorption onto novel chelating fibers. *Macromol. Rapid Commun.* **2002**, *23*, 535–539. [CrossRef]

55. Fatehi, M.; Shayegan, J.; Zabihi, M.; Goodarznia, I. Functionalized magnetic nanoparticles supported on activated carbon for adsorption of Pb(II) and Cr(VI) ions from saline solutions. *J. Environ. Chem. Eng.* **2017**, *5*, 1754–1762. [CrossRef]

56. Zhong, Q.Q.; Yue, Q.Y.; Gao, B.Y.; Li, Q.; Xu, X. A novel amphoteric adsorbent derived from biomass materials: Synthesis and adsorption for Cu(II)/Cr(VI) in single and binary systems. *Chem. Eng. J.* **2013**, *229*, 90–98. [CrossRef]

57. Dong, L.Y.; Liang, J.S.; Li, Y.; Hunang, S.Q.; Wei, Y.N.; Bai, X.; Jin, Z.H.; Zhang, M.; Qu, J.J. Effect of coexisting ions on Cr(VI) adsorption onto surfactant modified Auricularia auricula spent substrate in aqueous solution. *Ecotoxicol. Environ. Saf.* **2018**, *166*, 390–400. [CrossRef]

58. Wang, Y.; Liu, R.H. H_2O_2 treatment enhanced the heavy metals removal by manure biochar in aqueous solutions. *Sci. Total Environ.* **2018**, *628–629*, 1139–1148. [CrossRef]

59. Zhang, L.X.; Tang, S.Y.; He, F.X.; Liu, Y.; Mao, W.; Guan, Y.T. Highly efficient and selective capture of heavy metals by poly(acrylic acid) grafted chitosan and biochar composite for wastewater treatment. *Chem. Eng. J.* **2019**, *378*, 122215–122231. [CrossRef]

60. He, J.; Xue, H.X.; Lv, C.W.; Fan, Q.Y.; Liang, Y.; Sun, Y.; Shen, L.L.; Bai, S. The impacts of common ions on the adsorption of heavy metal. *Environ. Geol.* **2009**, *58*, 1499–1508. [CrossRef]

61. Wu, Z.D.; Zhao, C.; Zeng, W.G.; Wang, X.M.; Liu, C.F.; Yu, Z.Y.; Zhang, J.; Qiu, Z.M. Ultra-high selective removal of CR and Cr(VI) from aqueous solutions using polyethyleneimine functionalized magnetic hydrochar: Application strategy and mechanisms insight. *Chem. Eng. J.* **2022**, *448*, 137464. [CrossRef]